

Cite this: *Dalton Trans.*, 2019, **48**, 5263

Observation of a red Ce³⁺ center in SrLu₂O₄:Ce³⁺ phosphor and its potential application in temperature sensing

Sheng Zhang,^{a,b} Zhendong Hao,^{a*} Liangliang Zhang,^a Guo-Hui Pan,^a Huajun Wu,^a Hao Wu,^a Yongshi Luo,^a Xingyuan Liu,^{a,b} Hong Zhang,^c and Jiahua Zhang^{a,b*}

In Ce³⁺ activated SrLn₂O₄ type phosphors (Ln = Y, Lu, Sc, etc.) only one Ce³⁺ center was previously reported to show a blue emission band. In this paper, we report the observation of a second Ce³⁺ center in SrLu₂O₄:Ce³⁺. The new center shows a red emission band peaking at 600 nm with an excitation band at 485 nm. We attributed the new center (Ce(II)) to the substitution of the Lu³⁺ site and the original blue center (Ce(I)) to the substitution of the Sr²⁺ site. Spectroscopy studies indicate that Ce(I) centers are preferentially formed at a low doping concentration and the number ratio of Ce(I)/Ce(II) decreases with increasing Ce³⁺ concentration until beyond 0.002. The fluorescence lifetimes of the two centers were measured for various doping concentrations. Energy transfer from Ce(I) to Ce(II) was observed. It was found that the emission intensity of Ce(II) centers reduces much faster than that of Ce(I) with increasing temperature from 83 K up to 350 K, implying their potential application in temperature sensing based on their temperature dependent intensity ratios. A relative sensing sensitivity as high as 2.28% K⁻¹ at 283 K was achieved.

Received 21st February 2019,
Accepted 19th March 2019

DOI: 10.1039/c9dt00789j

rsc.li/dalton

Introduction

Among the present phosphors doped with rare-earth ions, Ce³⁺ ion activated phosphors are the most studied and have been extensively applied in field emission displays, white LEDs and scintillation.^{1–3} In addition to the high luminescence efficiency, another advantage of Ce³⁺-doped phosphors is that the luminescence color can be tuned from UV to the red region because of the sensitivity of the 5d energy position to the host lattice. For example, in different crystal field environments, Ce³⁺ ions can exhibit near UV-blue (peaking at ~427 nm), blue (peaking at ~445 nm), green (peaking at ~490 nm), yellow (peaking at ~550 nm), and red (peaking at ~620 nm) emissions in hosts Y₂SiO₅, Ba₂Y₅B₅O₁₇, Ba₉Lu₂Si₆O₂₄, Y₃Al₅O₁₂, and Sr₃Sc₄O₉, respectively.^{4–8} Therefore, Ce³⁺-doped phosphors with a specific emission color can be

designed *via* selecting a host with a special crystal field environment.

Rare-earth strontium oxides, SrLn₂O₄ (where Ln = Gd, Y, Sc, Lu, Ho, Er, Tm, Yb), with the space group *Pnam* were intensively studied for their magnetic properties in the past decades.^{9,10} Recently, a series of rare earth ion doped SrLn₂O₄ materials have been studied for application as phosphors because of their superior down/up-conversion characteristics. Eu³⁺-doped SrLu₂O₄ and SrGd₂O₄ luminescent materials have been studied and considered as promising red phosphors in solid state lighting devices.^{11,12} Eu²⁺ doped SrLu₂O₄ exhibited a broad red emission band centered at 610 nm and could be applied as an optical temperature sensor because of its strong thermal quenching.¹³

In the previous reports about SrLn₂O₄ type phosphors, the doped rare earth ions occupied Sr²⁺ or Ln³⁺ sites. SrY₂O₄:Ce³⁺ phosphor with an excitation of 410 nm shows blue emission peaking at 470 nm, and Ce³⁺ ions are considered to occupy Sr²⁺ sites.¹⁴ Another green phosphor SrSc₂O₄:Ce³⁺ shows 491 nm emission with great thermal stability, and Sr²⁺ ions are considered to be replaced by Ce³⁺ ions.¹⁵ Eu²⁺ doped SrSc₂O₄ phosphors show an emission band located in the deep red regions and Eu²⁺ ions are considered to substitute Sr²⁺ sites.¹⁶ In host SrLu₂O₄, Eu²⁺ ions are considered to occupy Sr²⁺ sites and it shows red emission with poor thermal stability.¹³ In

^aState Key Laboratory of Luminescence and Applications, Changchun Institute of Optics, Fine Mechanics and Physics, Chinese Academy of Sciences, 3888 Eastern South Lake Road, Changchun 130033, China.
E-mail: haozd@ciomp.ac.cn, zhangjh@ciomp.ac.cn

^bCenter of Materials Science and Optoelectronics Engineering, University of Chinese Academy of Sciences, Beijing 100049, China

^cVan't Hoff Institute for Molecular Sciences, University of Amsterdam, XH, Amsterdam, The Netherlands

SrLu₂O₄:Eu³⁺ phosphor, Eu³⁺ ions are considered to replace Lu³⁺ sites showing red emission.¹¹ Under 980 nm laser diode excitation, the SrLu₂O₄:Ho³⁺, Yb³⁺ phosphors exhibit an intense green upconversion emission band centered at 541 nm and weak red emission that peaked at 673 nm, and Songbin Liu *et al.* hold the view that Ho³⁺, Yb³⁺ ions occupied Lu³⁺ sites.¹⁷ The activator ions were all considered occupying only one site in the respective reports. In our previous work, we reported a blue phosphor, SrLu₂O₄:Ce³⁺, with great thermal stability and fabricated a white LED with a high color rendering index (CRI),¹⁸ and we also found that there were two luminescence centers in this phosphor and this phenomenon was not mentioned in the previous reports about SrLu₂O₄ type phosphors.

In this paper, a series of Ce³⁺ doped SrLu₂O₄ (SLO) phosphors were prepared *via* a conventional solid-state reaction technique. The host structure and the diffuse reflectance, excitation, and emission spectra of the samples were investigated in detail. The relationship and tendency of the two luminescence centers and occupying sites were discussed. The Ce(I) center shows great thermal stability while the emission of the Ce(II) center is quenched at room temperature. The values of relative sensitivity were also calculated and the results indicate this phosphor has potential in temperature sensing. Based on luminescence decay curves, lifetime and energy transfer efficiency have also been figured out. The energy transfer from Ce(I) to Ce(II) contributes to the red emission enhancement with increasing doping concentration.

Experimental

Material synthesis

SrLu_{2-x}O₄:xCe³⁺ samples were synthesized by a traditional high-temperature solid-state reaction. The constituent oxides and carbonates, SrCO₃ (A.R.), Lu₂O₃ (99.99%), and CeO₂ (99.99%), were employed as the raw materials. Powders were mixed according to the stoichiometric amounts of the formula of SrLu_{2-x}O₄:xCe³⁺ and Sr_{0.998}Lu₂O₄:0.002Ce³⁺ in their respective agate mortars and then placed in alumina crucibles. These crucibles were heated at 1600 °C for 6 hours in a reducing atmosphere (95% N₂/5% H₂), in order to reduce Ce⁴⁺ to Ce³⁺. After sintering, the powders were furnace-cooled naturally down to room temperature (RT). Finally, the as-prepared powders were washed with alcohol three times and dried at 60 °C for 6 hours in a drying oven to obtain the final phosphors.

Characterization

X-ray diffraction (XRD) patterns were obtained by using a powder diffractometer (Bruker, D8 Focus, Cu Kα, 40 kV, 40 mA). The XRD data were collected in the range of 15 to 70 degrees (2θ) with a count time of 2 s per step. Rietveld analysis was conducted using the computer software: FullProf program. The PL and photoluminescence excitation (PLE) spectra of Ce³⁺ ions were recorded by using a FL900 fluorometer with a xenon lamp

(Edinburg Instruments, UK). The temperature-dependent PL spectra were recorded on a fluorescence microscope (Olympus, BX53M) and CCD spectrometer (Ocean Optics). The decay curves were measured by using a FL910 fluorometer with 405 and 485 nm laser devices. All the measurements were conducted at room temperature unless specifically mentioned.

Results and discussion

In this work, all the samples were synthesized based on the substitution of Ce³⁺ for Lu³⁺ by charge balance and the pure crystal phases were acquired as shown in Fig. 1. The XRD patterns of SrLu₂O₄ and Sr(Lu_{1.998}Ce_{0.002})O₄ samples are in accordance with the standard data (JCPDS #32-1242). However, the diffraction peak of Lu₂O₃ locating at about 29.8° can be found as impurities in the patterns of (Sr_{0.998}Ce_{0.002})Lu₂O₄ samples. As we all know, multiple luminescence centers mean multiple occupations of sites, and Ce³⁺ ions occupy two sites in SrLu₂O₄ samples which causes a red emission to be observed besides the blue emission previously reported. In the presented reports, there were rare earth oxides left as impurities while raw materials were weighed according to the formula of Sr_{1-x}Ln₂O₄:xRe³⁺.⁹⁻¹⁷ The following explanations may contribute to the existence of rare oxides as impurities: Lu₂O₃ has low reactivity and is in excess in the raw materials according to the stoichiometric ratio of Sr_{1-x}Ln₂O₄:xRe³⁺. After sintering, the excess Lu₂O₃ in the raw materials is left as an impurity. According to the stoichiometric ratio, SrLu_{2-x}O₄:xCe³⁺ (x = 0–0.008), the excess of highly reactive SrCO₃ in the raw materials accelerated the solid-phase reaction and was volatilized completely after sintering with no impurities left. This is also the reason why we use the stoichiometric ratio of SrLu_{2-x}O₄:xCe³⁺ in this work to acquire pure phosphors though Ce³⁺ ions occupy both Sr²⁺ and Lu³⁺ sites.

In order to further understand the microstructure of the as-prepared samples, detailed Rietveld refinements and lattice parameters are performed shown in Fig. 2(a). The crystal

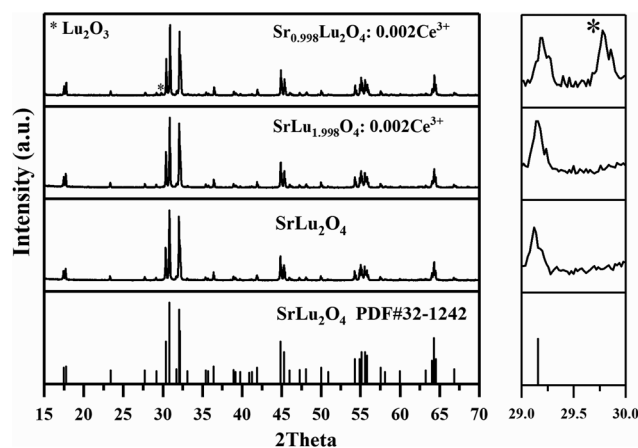


Fig. 1 The XRD of Sr_{0.998}Lu₂O₄:0.002Ce³⁺, SrLu_{1.998}O₄:0.002Ce³⁺, and SrLu₂O₄ samples and the standard XRD pattern of SrLu₂O₄ (JCPDS no. 32-1242) is included as a reference.

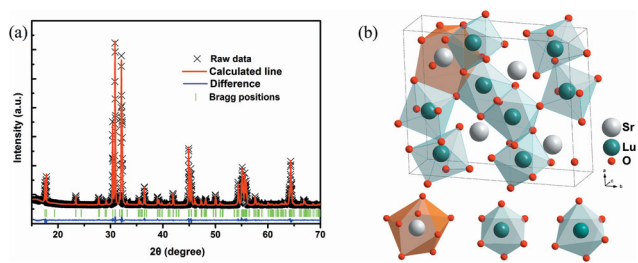


Fig. 2 (a) Rietveld refinements for SrLu_2O_4 . (b) Crystal structure schematic diagram of SrLu_2O_4 .

structure schematic diagram of SrLu_2O_4 is obtained according to the JCPDS card using Diamond software, shown in Fig. 2(b). The Sr^{2+} site is 8-coordinated with an average Sr–O bond length of 2.6145 Å and the ion radius is 1.26 Å, while the Lu site is 6-coordinated with an average Lu–O bond length of

2.2917 Å and 0.861 Å ion radius. The ion radius of Ce^{3+} is 1.01 Å for 6 coordination and 1.143 Å for 8 coordination. It means Sr^{2+} sites can provide larger space for Ce^{3+} ions to occupy though charge imbalance and this occupancy is also supported by previous reports.

As mentioned above, Ce^{3+} ions could occupy both Sr^{2+} and Lu^{3+} sites and two different luminescence centers have also been identified in Fig. 3(a). The Ce(I) center corresponds to the higher energy level which can be excited at 405 nm with emission at 460 nm; the Ce(II) center corresponds to the lower energy level which can be excited at 485 nm and shows an ultra-wide red emission band peaking at 600 nm. We used 390 nm excitation to get the full spectrum of Ce(I) emission shown in Fig. 3(a).

One can observe that the PLE band centered at 485 nm of Ce(II) entirely overlaps with the PL band of Ce(I), resulting in effective energy transfer from Ce(I) to Ce(II). The appearance of the strong Ce(I) PLE band at 405 nm in the PLE spectrum of

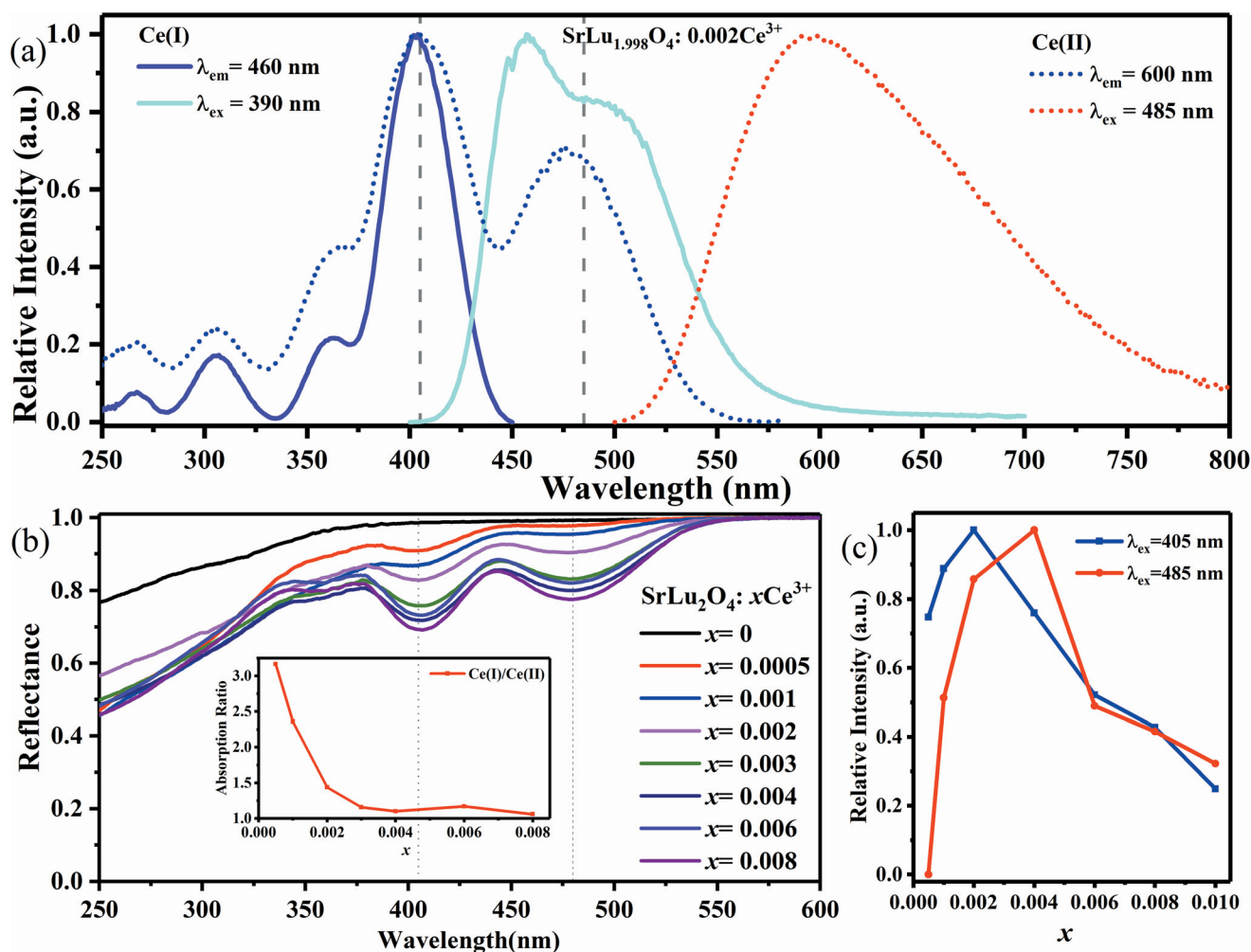


Fig. 3 (a) PLE and PL spectra of $\text{SrLu}_{1.998}\text{O}_4:0.002\text{Ce}^{3+}$ (full lines correspond to the Ce(I) center and dotted lines correspond to the Ce(II) center), and the dashed lines located at 405 nm and 485 nm as reference; (b) DR spectra of $\text{SrLu}_{2-x}\text{O}_4:x\text{Ce}^{3+}$ and the absorption rate of Ce(I)/Ce(II) around the dotted reference lines locating at 405 and 485 nm in the inset; (c) intensity variation of $\text{SrLu}_2\text{O}_4:x\text{Ce}^{3+}$ with varying Ce^{3+} concentrations excited at 405 nm and 485 nm.

Ce(II) is another strong piece of evidence of effective energy transfer. However, the Ce(II) emission is too weak to be discernible compared to that of the Ce(I) center under 405 nm excitation at room temperature whose intensity is lower than 10% of the Ce(I) emission. This is because Ce(II) is thermally quenched at room temperature and details will be discussed below.

According to the DR spectra in Fig. 3(b), the absorption in the range of 250–530 nm strengthened with increasing Ce³⁺ doping concentration. To observe the change of absorption of the two luminescence centers, the ratio of absorption of Ce(I)/(II) is also shown in the inset. The ratio is over 3.1 at first and decreases to nearly 1.1 with the Ce³⁺ concentration increasing beyond 0.002. It means Ce³⁺ ions tend to occupy Ce(I) center sites at a low doping concentration and both sites at a high doping concentration.

The dependence of emission intensity with changing concentration is also shown in Fig. 3(c). When $x = 0.0005$, the 600 nm emission nearly disappeared while the 460 nm emission reached a relatively high intensity. It also means Ce³⁺ ions tend to occupy the Ce(I) center at a low doping concentration. The 460 nm emission intensity reached the highest at $x = 0.002$ while the 600 nm emission intensity reached the highest at $x = 0.004$. This result also supports that Ce³⁺ ions tend to occupy the Ce(I) center and reaches quenching concentration with a lower doping concentration of Ce(I) center. After the quenching concentration, the emission intensities of both luminescence centers decrease rapidly.

Due to the energy transfer from Ce(I) to Ce(II), the low quenching concentration and large quenching distance were discussed in our former report.¹⁸ In addition, more details of the energy transfer between the two luminescence centers will be discussed below.

To better understand the two luminescence centers and energy transfer between them, the energy levels are also investigated. Based on the PLE spectra with different monitoring wavelengths, five excitation peaks were observed and shown as reference lines in Fig. 4(a). The excitation spectra and corresponding energy levels of SLO:Ce³⁺ are shown in Fig. 4.

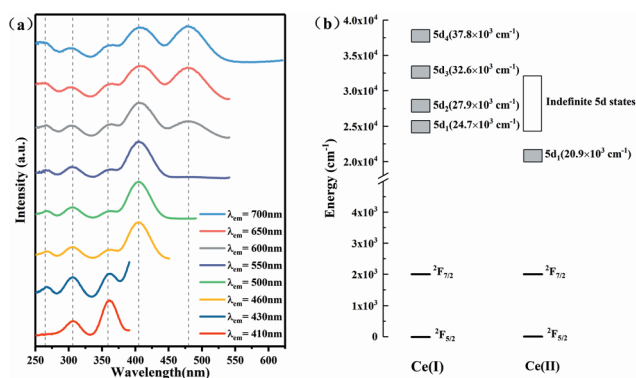


Fig. 4 (a) The PLE of SrLu_{1.998}O₄:0.002Ce³⁺ monitoring different wavelengths (λ_{em} = 410, 430, 460, 500, 550, 600, 650 and 700 nm) and dotted reference lines locating at 264, 306, 358, 405 and 485 nm; (b) the energy levels of Ce(I) and Ce(II) centers in SrLu_{1.998}O₄:0.002Ce³⁺.

Due to the energy transfer from Ce(I) to Ce(II), the 5d₁ level of Ce(II) can be identified locating at 20.9 × 10³ cm⁻¹ while the other 5d levels can be indefinite for the Ce(II) center according to the excitation band of Ce(I) center.

We discerned that the Ce(I) center corresponds to Ce³⁺ ions occupying Sr²⁺ sites while the Ce(II) center corresponds to Ce³⁺ ions occupying Lu³⁺ sites and the details are discussed as follows. According to the ionic radius, Ce³⁺ ions (CN = 6, $r = 1.01$ Å; CN = 8, $r = 1.14$ Å) could occupy both Sr²⁺ (CN = 8, $r = 1.26$ Å) and Lu³⁺ (CN = 6, $r = 0.861$ Å) sites. The r change is 9.5% for occupying the Sr²⁺ site and 17.3% for occupying the Lu³⁺ site. This means that Ce³⁺ ions tend to occupy Sr²⁺ sites instead of Lu³⁺ sites at a low Ce³⁺ doping concentration because of less lattice distortion. With increasing doping concentration, charge mismatch promotes the occupation of Lu³⁺ sites. Due to the serious distortion of CeO₆ polyhedra, the electron–phonon coupling strengthens, which leads to the ultra-wide emission band of the Ce(II) center.

According to the van Uitert formula,

$$E = Q \left[1 - \left(\frac{V}{4} \right)^{\frac{1}{V}} \times 10^{-\frac{n \times E_a \times r}{80}} \right] \quad (1)$$

where E signifies the emission peak position of Ce³⁺ ions, Q signifies the energy for the lowest d-band edge of the free Ce³⁺ ($Q = 50\,000$ cm⁻¹), V signifies the valence of the ion ($V = 3$ for Ce³⁺), n signifies the number of anions in the immediate shell about the Ce³⁺, r signifies the radius (Å) of the cation replaced by the Ce³⁺, and E_a signifies the electron affinity of the atoms that form anions (eV). For SrLu_{1.998}O₄:0.002Ce³⁺, the values of n and r with Ce³⁺ occupying Sr²⁺ sites are bigger than those with Ce³⁺ occupying Lu³⁺ sites. This means that the emission peak of Ce³⁺ occupying Sr²⁺ sites is smaller in wavelength.

Covalent bond theory and crystal field theory are often used to explain the red/blue shift in excitation and emission spectra caused by co-doped ions. Here they can also help determine the specific occupation of Ce³⁺ ions.

According to the formula:

$$D_q = \frac{Ze^2r^4}{6R^5} \quad (2)$$

where Z and e are the charge of the anion and electron, respectively, r is the radius of the d wave function, and R is the bond length. For SrLn₂O₄:Ce³⁺ phosphors, the bond length of Sr–O in SrSc₂O₄ (2.6041 Å) and SrY₂O₄ (2.5698 Å) is very close to that in SrLu₂O₄ (2.6145 Å). It means that the crystal field would split while Ce³⁺ ions occupy Sr²⁺ sites and lead to nearly the same Stokes shift. In the previous reports about phosphors with the same configuration and excitation peak locating at about 410 nm, Ce³⁺ ions were all considered to occupy Sr²⁺ sites. What's more, the value of the Stokes shift of the Ce(I) center is 55 nm which is very close to that in SrLn₂O₄ type phosphors while it is much smaller than that of the Ce(II) center (115 nm) as shown in Table 1. For the Ce(II) center, the bigger Stokes shift means stronger electron–phonon coupling which leads to a broader red emission band.

Table 1 PLE and occupying situation in SrLu₂O₄ type phosphors

Formula	λ_{ex}/nm	λ_{em}/nm	$\Delta S/\text{nm}$	Replaced sites	Ref.
SrSc ₂ O ₄ :Ce ³⁺	432	491	61	Sr ²⁺	15
SrY ₂ O ₄ :Ce ³⁺	410	470	60	Sr ²⁺	14
SrLu ₂ O ₄ :Ce ³⁺	405	460	55	Sr ²⁺	This work
SrLu ₂ O ₄ :Ce ³⁺	485	600	115	Lu ³⁺	This work

As shown in Fig. 5, the temperature-quenching properties of SrLu_{2-x}O₄:xCe³⁺ ($x = 0.0005, 0.002, \text{ and } 0.008$) at the two luminescence centers were also studied. For $x = 0.0005$ and 0.002 , the sample kept nearly 50% of the strongest emission at a high temperature as shown in Fig. 5(a) and (b). For $x = 0.008$, the red emission cannot be neglected at low temperature as shown in Fig. 5(c). In consideration of the energy transfer from Ce(I) to Ce(II), the emission was measured with excitation at both 405 and 485 nm at the same temperature. The independent Ce(II) emission can be separated from the 405 nm-excitation emission according to the peak of the 485 nm-excitation emission, and then become the independent Ce(I) emission. For the Ce(I) center, SLO:Ce³⁺ shows stability in the whole temperature range and the stability decreases with increasing Ce³⁺ concentration.

The measured data lines could not be fitted well with the Arrhenius curves and it meant a complicated luminescence process had happened with increasing temperature. For $x = 0.008$, there exist numerous Ce(I), Ce(II) centers and energy transfers between them. With increasing temperature, the energy transfer from Ce(I) to Ce(II) became more efficient.

For the Ce(II) center, the intensity was too weak while $x = 0.0005$ and the background effect would be equal to the luminescence of phosphors because of the restriction of the measuring device. Therefore, we focused on the luminescence properties of Ce(II) while $x = 0.002$ and 0.008 .

The stability of the luminescence at the Ce(II) center was quite bad and the luminescence was quenched rapidly with increasing temperature and showed a weak PL at room temperature. This also explained the reason why the Ce(II) center emission is too weak compared to Ce(I) with nearly the same strong absorbance.

To better understand the temperature dependence of the photoluminescence, the activation energy was calculated using the Arrhenius equation given as

$$I(T) = \frac{I_0}{1 + Ae^{-E_a/k_B T}} \quad (3)$$

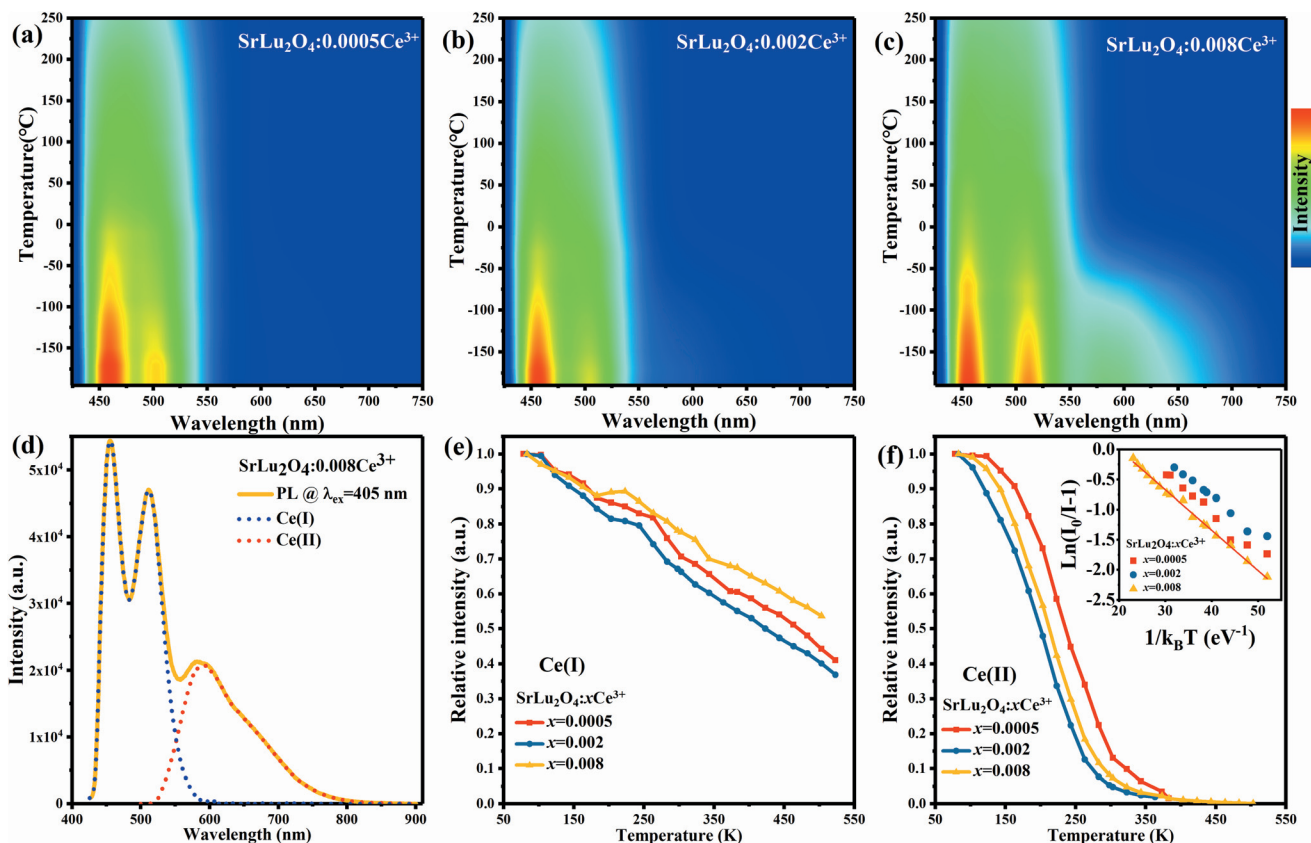


Fig. 5 (a–c) Temperature-dependent photoluminescence measurements of the emission spectrum of SrLu_{2-x}O₄:xCe³⁺ ($x = 0.0005, 0.002, \text{ and } 0.008$); (d) the PL of SrLu₂O₄:0.008Ce³⁺ excited by 405 nm at 78 K. The emission spectra is fit to display the two center curves (blue and red dot); temperature dependence of the integrated emission intensities in SrLu_{2-x}O₄:xCe³⁺ ($x = 0.0005, 0.002, \text{ and } 0.008$) at Ce(I) (e) and Ce(II) (f) centers, and the Arrhenius analyses are inset.

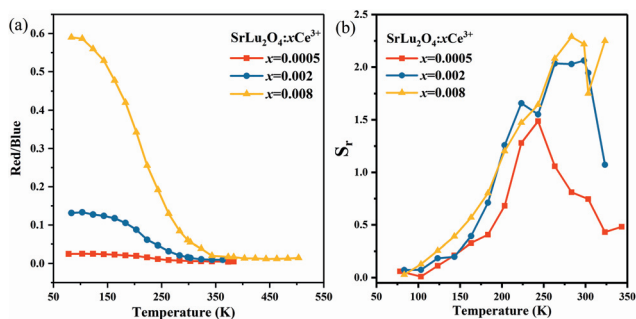


Fig. 6 (a) The ratio of red/blue emission intensity vs. temperature; (b) relative sensitivity (S_r) of the temperature of $\text{SrLu}_{2-x}\text{O}_4:\text{xCe}^{3+}$ ($x = 0.0005, 0.002, \text{ and } 0.008$).

$$\ln\left(\frac{I_0}{I(T)} - 1\right) = \ln A - \frac{E_a}{k_B T} \quad (4)$$

where I_0 is the PL intensity at 0 K, here it is treated as the one at 90 K if the PL intensity is stable at the liquid nitrogen temperature, $I(T)$ is the PL intensity at a given temperature T , A is a constant, E_a is the activation energy for thermal quenching, and k_B is the Boltzmann constant. For the Ce(II) center, the experimental data are well fitted using eqn (4), as shown in the inset in Fig. 5(f). The value of E_a was found to be 0.067 eV for $x = 0.008$. This value is very small and explains the bad thermal stability. The non-radiation transition happened easily for ions in excited states with a low activation energy.

The two luminescence centers showed a huge difference in thermal stability and the ratio of emission of the two centers could be applied in temperature sensing. In the previous reports, temperature sensing research studies focused on upconversion, and the emissions of different energy levels were studied. In this paper, the emission of two centers is set as a subject and the $\text{SrLu}_{1.992}\text{O}_4:0.008\text{Ce}^{3+}$ sample was chosen for its bright red luminescence. The emission intensity ratio between Ce(I) and Ce(II), defined as FIR ($I_{\text{Ce(II)}}/I_{\text{Ce(I)}}$), is adopted to study the temperature-dependent luminescence properties, shown in Fig. 6(a), and the relative sensitivities (S_r) are also analyzed in Fig. 6(b). The value of FIR and S_r can be established and expressed as

$$\text{FIR} = \frac{I_{\text{Ce(II)}}}{I_{\text{Ce(I)}}} = \frac{I_{\text{Red}}}{I_{\text{Blue}}} \quad (5)$$

$$S_r = \left| \frac{1}{\text{FIR}} \times \frac{\partial \text{FIR}}{\partial T} \right| \times 100\% \quad (6)$$

Due to the Ce(II) center being quenched at 350 K, the value of FIR is accurate at the temperature below 300 K, and S_r maintains a high value in the temperature range of 150–300 K. S_r increases firstly then decreases with increasing temperature, and the maximum is 2.28% K^{-1} at 283 K. Compared to the recent reports, Table 2, $\text{SrLu}_2\text{O}_4:\text{Ce}^{3+}$ is a promising candidate for optical temperature sensors with high sensitivity in the range of 150–300 K.

Table 2 Maximal relative sensitivities of typical lanthanide ion doped materials in previous reports

Rare-earth ions	Host	Temperature range (K)	S_r (% K^{-1})	Ref.
Er^{3+}	$\text{Na}_{0.82}\text{Ca}_{0.08}\text{Er}_{0.16}\text{Y}_{0.853}\text{F}_4$	5–300	0.22	22
$\text{Ho}^{3+}, \text{Yb}^{3+}$	Y_2O_3	10–300	0.97	23
$\text{Er}^{3+}, \text{Yb}^{3+}$	Y_2O_3	93–613	0.44	24
$\text{Ho}^{3+}, \text{Yb}^{3+}$	$\text{Ba}_{0.77}\text{Ca}_{0.23}\text{TiO}_3$	93–300	0.53	25
Pr^{3+}	$\beta\text{-NaYF}_4$	120–300	0.73	26
Ce^{3+}	SrLu_2O_4	150–300	2.28	This work
$\text{Er}^{3+}, \text{Yb}^{3+}$	$\text{Bi}_7\text{Ti}_4\text{NbO}_{21}$	153–553	0.44	27
$\text{Er}^{3+}, \text{Yb}^{3+}$	$\beta\text{-NaYF}_4$	160–300	1.20	28
$\text{Tm}^{3+}, \text{Yb}^{3+}$	YOF	190–300	0.84	29
$\text{Er}^{3+}, \text{Yb}^{3+}$	$\text{Ba}_5\text{Gd}_8\text{Zn}_4\text{O}_{21}$	200–490	0.32	30
$\text{Dy}^{3+}, \text{Yb}^{3+}$	$\text{Y}_4\text{Al}_2\text{O}_9$	273–1273	0.67	31
$\text{Ce}^{3+}, \text{Tb}^{3+}$	LaOBr	293–433	0.42	32
$\text{Eu}^{3+}, \text{Eu}^{2+}$	$\text{Ca}_8\text{ZrMg}(\text{PO}_4)_6(\text{SiO}_4)$	293–473	5.94	33
Er^{3+}	$\text{Ca}_2\text{Gd}_8(\text{SiO}_4)_6\text{O}_2$	293–553	1.14	34
$\text{Er}^{3+}, \text{Yb}^{3+}$	Gd_2O_3	298–723	0.84	35
$\text{Er}^{3+}, \text{Yb}^{3+}$	$\text{NaY}(\text{MoO}_4)_2$	303–523	0.97	36
$\text{Tb}^{3+}, \text{Eu}^{3+}$	$\beta\text{-NaYF}_4$	303–563	1.17	37
$\text{Ce}^{3+}, \text{Tb}^{3+}, \text{Eu}^{3+}$	$\beta\text{-NaYF}_4$	300–573	0.46	38

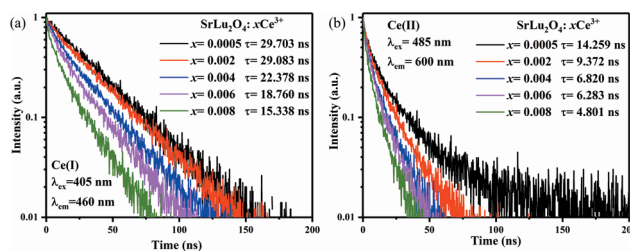


Fig. 7 The decay curves of the two luminescence centers were excited by 405 nm and 485 nm laser devices and monitored at 460 and 600 nm at room temperature, and the calculated lifetimes are also listed.

Table 3 The lifetime and ET efficiency of two luminescence centers with the Ce^{3+} concentration were calculated

Concentration (x)	Lifetime1 (τ_1)/ns	ET efficiency (η)	Lifetime2 (τ_2)/ns
0.0005	29.703		14.259
0.002	29.083	0.020873	9.372
0.004	22.378	0.246608	6.82
0.006	18.76	0.368414	6.283
0.008	15.338	0.483621	4.801

The decay curves of the two luminescence centers in the $\text{SrLu}_2\text{O}_4:\text{xCe}^{3+}$ ($x = 0.0005\text{--}0.008$) were measured and are shown in Fig. 7, and the lifetimes (τ) were also calculated according to the formula:

$$\bar{\tau} = \frac{\int_0^{\infty} I(t)tdt}{\int_0^{\infty} I(t)dt} \quad (7)$$

where $I(t)$ stands for the emission intensity of the Ce^{3+} ions at time t , and the average decay times were calculated and are listed in Table 3. The lifetime decrease with increasing Ce^{3+} concentration is due to the lattice distortion and energy trans-

fer in a single luminescence center. For $x = 0.0005$, Ce^{3+} ions mainly occupied Sr^{2+} sites corresponding to the Ce(I) center and both luminescence centers showed quite a long lifetime, and the values are 29.7 and 14.3 ns. For $x > 0.002$, both of luminescence centers were up to the quenching concentrations and showed shorter lifetimes. Generally, the lifetime of Ce^{3+} in the blue phosphor with 8 coordination is about 35 ns and remains about 20 ns with increasing doping concentration.^{19–21} The existence of the Ce(II) center is attributed to a lower τ_1 with a higher doping concentration.

To investigate the energy transfer between the two luminescence centers, the energy transfer efficiency (η) can be calculated from the decay lifetime by using the equation,

$$\eta = 1 - \frac{\tau}{\tau_0} \quad (8)$$

where τ is the lifetime of Ce^{3+} emission and τ_0 is the one corresponding to the lowest doping concentration. The calculated results are shown in Fig. 7 and Table 3. For $x = 0.002$, η is so small that the energy transfer can be ignored. This result also supports the point that Ce(I) centers are preferentially formed at a low doping concentration. For $x = 0.004$, the value of η increases to 0.25 and it is the quenching concentration for the Ce(II) center. Energy transfer from Ce(I) to Ce(II) contributes to the enhancement of red emission with increasing doping concentration.

Conclusions

The spectroscopic properties of a series of $\text{SrLu}_{2-x}\text{O}_4:x\text{Ce}^{3+}$ phosphors ($x = 0.0005\text{--}0.008$) in the near UV-cyan range were investigated systematically. A new red luminescence center was observed in SrLu_2O_4 type phosphors. According to the ion radius, van Uitert formula, crystal field theory and reports on other SrLu_2O_4 type phosphors, Ce^{3+} ions occupying Sr^{2+} sites correspond to the Ce(I) center while those occupying Lu^{3+} sites correspond to Ce(II) centers. Based on the excitation spectra of $\text{SrLu}_{2-x}\text{O}_4:x\text{Ce}^{3+}$, the observed excitation bands of Ce(I) in Ce(II) excitation mean efficient energy transfer from Ce(I) to Ce(II) and crystal-field split 5d states are located at 265, 306, 358, 404 and 485 nm. Ce^{3+} ions preferentially occupy Sr^{2+} sites at low doping concentrations, and they start to occupy the Lu^{3+} sites when the Ce^{3+} concentration increases beyond 0.002 according to the DR spectra. Ce(I) center shows better thermal stability while the Ce(II) center is quenched at room temperature. The huge difference in thermal stability between the two luminescence centers could be applied in temperature sensing, and the maximal S_r is 2.28% K^{-1} at 150–300 K. In $\text{SrLu}_{1.9995}\text{O}_4:0.0005\text{Ce}^{3+}$, the emission of the short-wavelength Ce(I) centers has a decay time of about 30 ns, while that of the long-wavelength Ce(II) centers is 14 ns. The strong thermal quenching of the Ce(II) center and energy transfer between the two luminescence centers lead to the low quenching concentration of the Ce(I) center.

Conflicts of interest

There are no conflicts to declare.

Acknowledgements

This work was partially supported by National Natural Science Foundation of China (Grant No. 51772286, 11874055 and 11604330), National Key R&D Program of China (Grant No. 2016YFB0400605, 2016YFB0701003, 2017YFB0403104), Natural Science Foundation of Jilin province (Grant No. 20160520171JH).

References

- 1 Y. Wei, G. Xing, K. Liu, G. Li, P. Dang, S. Liang, M. Liu, Z. Cheng, D. Jin and J. Lin, *Light: Sci. Appl.*, 2019, **8**, 15.
- 2 L. Y. Feng, Z. D. Hao, X. Zhang, L. L. Zhang, G. H. Pan, Y. S. Luo, L. G. Zhang, H. F. Zhao and J. H. Zhang, *Dalton Trans.*, 2015, **45**, 1539.
- 3 Q. Bao, Z. Wang, J. Sun, Z. Wang, X. Meng, K. Qiu, Y. Chen, Z. Yang and P. Li, *Dalton Trans.*, 2018, **47**, 13913–13925.
- 4 Y. Parganiha, J. Kaur, V. Dubey and K. V. R. Murthy, *Mater. Sci. Semicond. Process.*, 2015, **31**, 715–719.
- 5 X. Yu, Z. Hao, L. Zhang, W. Xiao, W. Dan, Z. Xia, G. H. Pan, Y. Luo and J. Zhang, *Inorg. Chem.*, 2017, **56**, 4538–4544.
- 6 Y. Liu, J. Zhang, C. Zhang, J. Xu, G. Liu, J. Jiang and H. Jiang, *Adv. Opt. Mater.*, 2015, **3**, 1096–1101.
- 7 G. Blasse and A. Bril, *Appl. Phys. Lett.*, 1967, **11**, 53–55.
- 8 T. Hasegawa, W. K. Sun, T. Ueda, T. Ishigaki, K. Uematsu, H. Takaba, K. Toda and M. Sato, *J. Mater. Chem. C*, 2017, **5**, 9472–9478.
- 9 H. Karunadasa, Q. Huang, B. Ueland, J. Lynn, P. Schiffer, K. Regan and R. Cava, *Phys. Rev. B: Condens. Matter Mater. Phys.*, 2005, **71**, 144414.
- 10 B. Malkin, S. Nikitin, I. Mumdzhi, D. Zverev, R. Yusupov, I. Gilmudinov, R. Batulin, B. Gabbasov, A. Kiiamov and D. Adroja, *Phys. Rev. B: Condens. Matter Mater. Phys.*, 2015, **92**, 094415.
- 11 L. Zhou, J. Shi and M. Gong, *Mater. Res. Bull.*, 2005, **40**, 1832–1838.
- 12 J. Singh and J. Manam, *Ceram. Int.*, 2016, **42**, 18536–18546.
- 13 K.-H. Kim, E.-H. Kang, B.-K. Kang, K. P. Kim and S.-H. Hong, *J. Lumin.*, 2017, **183**, 13–16.
- 14 V. Manivannan, H. A. Comanzo, A. A. Setlur, A. M. Srivastava, P. A. Schmidt and U. Happek, *J. Lumin.*, 2003, **102–103**, 635–637.
- 15 G. Li, Y. Fan, H. Guo and Y. Wang, *New J. Chem.*, 2017, **41**, 5565–5571.
- 16 J. Zhao, X. Sun and Z. Wang, *Chem. Phys. Lett.*, 2018, **691**, 68–72.
- 17 S. Liu, X. Ye, S. Liu, M. Chen, H. Niu, D. Hou and W. You, *J. Am. Ceram. Soc.*, 2017, **100**, 3530–3539.
- 18 S. Zhang, Z. Hao, L. Zhang, G. H. Pan, H. Wu, X. Zhang, Y. Luo, L. Zhang, H. Zhao and J. Zhang, *Sci. Rep.*, 2018, **8**, 10463.

- 19 Y. Luo, Z. Xia, H. Liu and Y. He, *Opt. Mater.*, 2014, **36**, 723–726.
- 20 X. Zhang, J. Song, C. Zhou, L. Zhou and M. Gong, *J. Lumin.*, 2014, **149**, 69–74.
- 21 X. Zhang, Z.-C. Wu, Y. Li, J. Xu and L. Tian, *Dyes Pigm.*, 2017, **144**, 94–101.
- 22 X. Wang, Q. Liu, Y. Bu, C.-S. Liu, T. Liu and X. Yan, *RSC Adv.*, 2015, **5**, 86219–86236.
- 23 K. Zheng, Z. Liu, C. Lv and W. Qin, *J. Mater. Chem. C*, 2013, **1**, 5502–5507.
- 24 P. Du, L. Luo, Q. Yue and W. Li, *Mater. Lett.*, 2015, **143**, 209–211.
- 25 P. Du, L. Luo and J. S. Yu, *J. Alloys Compd.*, 2015, **632**, 73–77.
- 26 S. Zhou, G. Jiang, X. Wei, C. Duan, Y. Chen and M. Yin, *J. Nanosci. Nanotechnol.*, 2014, **14**, 3739–3742.
- 27 H. Zou, J. Li, X. Wang, D. Peng, Y. Li and X. Yao, *Opt. Mater. Express*, 2014, **4**, 1545–1554.
- 28 S. Zhou, K. Deng, X. Wei, G. Jiang, C. Duan, Y. Chen and M. Yin, *Opt. Commun.*, 2013, **291**, 138–142.
- 29 H. Lu, J. Yang, D. Huang, Q. Zou, M. Yang, X. Zhang, Y. Wang and H. Zhu, *J. Lumin.*, 2019, **206**, 613–617.
- 30 H. Suo, C. Guo and T. Li, *J. Phys. Chem. C*, 2016, **120**, 2914–2924.
- 31 Z. Boruc, M. Kaczkan, B. Fetlinski, S. Turczynski and M. Malinowski, *Opt. Lett.*, 2012, **37**, 5214–5216.
- 32 X. Zhang, Y. Huang and M. Gong, *Chem. Eng. J.*, 2017, **307**, 291–299.
- 33 F. Ruan, D. Deng, M. Wu, B. Chen, L. Lei, R. Lei and S. Xu, *J. Alloys Compd.*, 2019, 1153–1161.
- 34 J. Zhang, G. Chen, Z. Zhai, H. Chen and Y. Zhang, *J. Alloys Compd.*, 2019, **771**, 838–846.
- 35 Y. Tian, B. Tian, P. Huang, L. Wang and B. Chen, *RSC Adv.*, 2015, **5**, 14123–14128.
- 36 X. Yang, Z. Fu, Y. Yang, C. Zhang, Z. Wu and T. Sheng, *J. Am. Ceram. Soc.*, 2015, **98**, 2595–2600.
- 37 M. Ding, M. Xu and D. Chen, *J. Alloys Compd.*, 2017, **713**, 236–247.
- 38 M. Ding, H. Zhang, D. Chen, Q. H. J. Xi and Z. Ji, *J. Alloys Compd.*, 2016, **672**, 117–124.